

# New derivatives of hydantoin as potential antiproliferative agents: biological and structural characterization in combination with quantum chemical calculations

Sleem Hmuda · Nemanja Trišović · Jelena Rogan · Dejan Poleti ·  
Željko Vitnik · Vesna Vitnik · Nataša Valentić · Biljana Božić ·  
Gordana Ušćumlić

Received: 24 September 2013 / Accepted: 26 December 2013  
© Springer-Verlag Wien 2014

**Abstract** Two new series of hydantoin derivatives, 3-(4-substituted benzyl)-5,5-diphenyl- and 3-(4-substituted benzyl)-5-ethyl-5-phenylhydantoins, were synthesized and their antiproliferative activity was tested against human colon cancer HCT-116 and breast cancer MDA-MB-231 cell lines. The presence of different substituents on both hydantoin and benzyl moieties changed the antiproliferative activity of the investigated hydantoins, whereby most of the compounds showed superior antiproliferative activity against MDA-MB-231 than against the HCT-116 cell line. The structure of three compounds was studied by single-crystal X-ray diffraction. The general structural characteristic is the presence of N–H···O hydrogen bonds in crystal packings. The molecular geometry and bonding features of the investigated hydantoins in the ground states were calculated using the density functional method. The relationship between structure and antiproliferative activity was discussed. The data presented in this investigation afford guidelines for the preparation of new hydantoin derivatives with greater antiproliferative activity.

**Electronic supplementary material** The online version of this article (doi:10.1007/s00706-013-1149-6) contains supplementary material, which is available to authorized users.

S. Hmuda · N. Trišović · J. Rogan · D. Poleti · N. Valentić ·  
G. Ušćumlić (✉)  
Faculty of Technology and Metallurgy, University of Belgrade,  
Belgrade, Serbia  
e-mail: goca@tmf.bg.ac.rs

Ž. Vitnik · V. Vitnik  
Department of Chemistry, IChTM-Institute of Chemistry,  
Technology and Metallurgy, University of Belgrade,  
Belgrade, Serbia

B. Božić  
Faculty of Biology, University of Belgrade, Belgrade, Serbia

**Keywords** Hydantoin · Antiproliferative activity · X-ray structure determination · Quantum chemical calculations · Natural bond orbital analysis

## Introduction

Derivatives of hydantoin (imidazolidine-2,4-dione) represent pharmacologically important compounds that are employed, among other uses, as anticonvulsants, antiarrhythmics, antimicrobial agents, and skeletal muscle relaxants [1]. Phenytoin (5,5-diphenylhydantoin) is an example of a well-known drug that was introduced in the treatment of epilepsy in the late 1930s, but its versatile biological effects still attract considerable attention within the scientific community.

Some hydantoin derivatives have already been identified as antitumor agents. Spiromustine, a spirohydantoin mustard, rapidly penetrates the blood–brain barrier and directs the drug delivery to brain tumors [2]. On the other side, nilutamide [3-(4-nitro-3-trifluoromethylphenyl)-5,5-dimethylhydantoin] is a potent antiandrogen used primarily in the treatment of prostate cancer in advanced stages [3]. Lipophilic derivatives of hydantoin bearing cycloalkyl, phenyl, or benzhydryl substituents show inhibitory activity against several cancer cell lines [4]. The antiproliferative effects of diazaspiro bicyclo hydantoins have been determined on the human leukemia cell lines K562 and CEM [5]. It has been demonstrated that the cytotoxic activity of the compounds with a substituent in position 3 increases in the order: alkene > ester > ether. Fluorinated spirohydantoins have been reported to induce cytotoxicity in chronic myelogenous leukemia by inhibiting the cell growth via interfering with DNA replication [6]. 1-(2-Arylethyl)-5-arylidenehydantoins inhibit the proliferation of the lung cancer cell line A549 via a dual mechanism: blocking

EGFR tyrosine kinase activity and inducing genomic DNA damage [7]. 5-Arylidenehydantoin shows potent *in vitro* and *in vivo* antiproliferative and anti-invasive properties against the prostate cancer cell line PC-3M [8]. A  $\beta$ -carboline hydantoin has been found to inhibit phosphodiesterase 5 and the proliferation of the colon cancer cell line HC-29 [9].

3-(2-Oxo-2-arylethyl)-5,5-diphenylhydantoin derivatives have recently been reported to possess selective activity against the renal cancer cell lines A498 and UO-31, whereby the derivative bearing the piperidine moiety shows additionally strong activity against melanoma and breast cancer cell lines MDA-MB-435 and MCF7, respectively [10]. Molecular docking of the most active compound into the active sites of EGFR and V600E-B-RAF kinase has also been studied. It has been demonstrated that the hydantoin ring binds in the enzyme-active site through the formation of hydrogen bonds, while the phenyl groups in position 5 are responsible for the arene  $\pi$ - $\pi$  interactions. We have previously shown that in a series of 3-alkyl-5,5-diphenylhydantoin derivatives, the derivative with a benzyl group has a significant antiproliferative effect on the colon cancer cell line HCT-116 [11]. This compound also exhibits antibacterial activity against the Gram-positive bacterium *Enterococcus faecalis* and the Gram-negative bacteria *Escherichia coli* ATCC 25922 and *Escherichia coli* (clinically isolated). Using 3-benzyl-5,5-diphenylhydantoin as a leading compound, the present research has been focused on the effects of structural modifications on both hydantoin and benzyl moieties on the antiproliferative activity.

In this study, two series of 3-(4-substituted benzyl)-5,5-diphenyl- and 3-(4-substituted benzyl)-5-ethyl-5-phenylhydantoin derivatives (Fig. 1) have been synthesized and their antiproliferative activity has been evaluated against cell lines MDA-MB-231 (human breast adenocarcinoma) and HCT-116 (human colon cancer), as well as non-cancerous, normal rat peritoneal macrophage controls. This has further motivated a detailed theoretical analysis of substituent effects on the geometry, electronic structure, and frontier molecular orbitals (MOs) of the investigated hydantoin derivatives. The stability of compound **2a** arising from hyperconjugative interactions and charge delocalization has been studied by using natural bond orbital (NBO)

analysis. In addition, the X-ray crystal structure determination for compounds **2a**, **2e**, and **2g** is presented.

## Results and discussion

### Antiproliferative activity

Cytotoxic evaluation has been the first step in the biological characterization of the investigated compounds. The examination of cytotoxic effects (non-specific cell killing) on the viability of unstimulated and lipopolysaccharide (LPS)-stimulated rat peritoneal macrophages has been conducted by MTT assay. All investigated hydantoin derivatives are non-toxic to normal rat peritoneal macrophages (data not shown).

The antiproliferative activity of compounds **1a–1h** and **2a–2g** has been tested against cancer cell lines HCT-116 and MDA-MB-231. With the exception of compounds **1d** (0.1 and 0.01  $\mu\text{mol dm}^{-3}$ ) and **1h** (1 and 0.1  $\mu\text{mol dm}^{-3}$ ), all compounds exhibit significant antiproliferative effects against human breast cancer cells MDA-MB-231 in the investigated concentration range (Table S1 in Supplementary Material). As can be seen, the highest antiproliferative activity has been observed by compounds **1b–1d** and **1h** against MDA-MB-231. These compounds show a better antiproliferative activity with respect to the unsubstituted derivative **1a** (Fig. 2). Furthermore, 5,5-diphenylhydantoin derivatives (series **1**) exhibit a higher antiproliferative activity when compared to 5-ethyl-5-phenylhydantoin derivatives (series **2**). This may be attributed, at first sight, to the introduction of the additional phenyl group in position 5, which contributes to the formation of a strong lipophilic shield around the hydantoin moiety. Concerning the compounds with an alkyl group as the benzyl substituent X, compound **1b** with the methyl group shows less than 50 % inhibition of MDA-MB-231 cell proliferation in the highest concentration (100  $\mu\text{mol dm}^{-3}$ ) and has a better effect when compared to the compound **1h** with the *tert*-butyl group. Compounds having a halogen substituent as X (**1c**: X = Cl; **1d**: X = Br) have a superior antiproliferative capacity than the other compounds in series **1**.

Compounds **1a–1h** and **2a–2f** exhibit significant antiproliferative activity against the human colon cancer cells HCT-116 only in the highest investigated concentration (100  $\mu\text{mol dm}^{-3}$ ), and this inhibition is lower compared to the inhibition of cells in MDA-MB-231 (Fig. 2 and Table S2 in Supplementary Material). The strongest antiproliferative activity has been observed by compounds **1b** and **1c**.

It can be concluded that all investigated hydantoin derivatives show satisfying inhibitory activity against the investigated cancer cell lines without non-specific

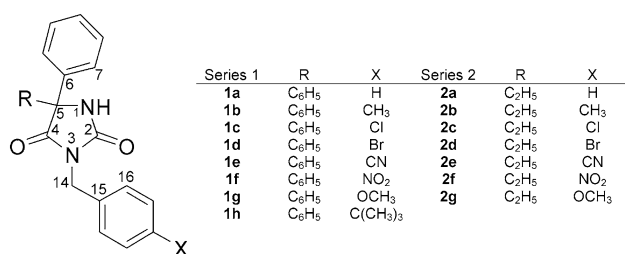
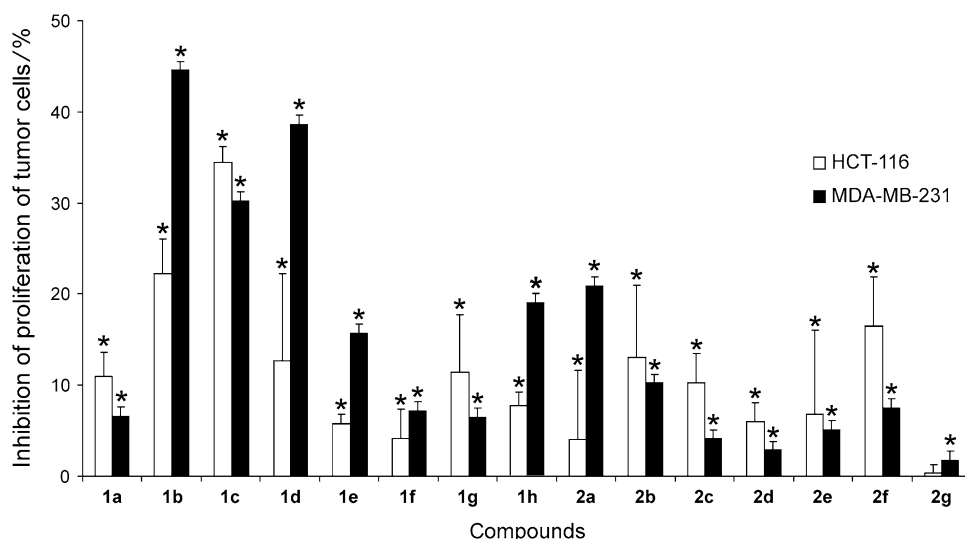


**Fig. 1** Chemical structures of the investigated hydantoin derivatives

**Fig. 2** The effect of the investigated hydantoin at the concentration of  $100 \mu\text{mol dm}^{-3}$  on the inhibition of proliferation HCT-116 and MDA-MB-231 cell lines (\* $p < 0.05$  vs non-treated cells)



cytotoxic effect. Because the investigated compounds are non-toxic to normal rat peritoneal cells, the pronounced antiproliferative activity against MDA-MB-231 indicates their significant anticancer potential for breast cancer cells. Also, the results of this study indicate a better antiproliferative potential of 5,5-diphenylhydantoin bearing an alkyl (methyl or *tert*-butyl) or halogen substituent in the benzyl moiety. In particular, compounds **1b**, **1c**, and **1d** may represent good starting points for the development of new, specific antiproliferative hydantoin. It has been reported that compounds **1c** and **1g** show significant inhibition of the renal cancer cell lines (A498 and UO-31, 31–59 % at the concentration of  $10 \mu\text{mol dm}^{-3}$ ) [10], while the replacement of the benzyl moiety with a phenacyl group results in derivatives with somewhat decreased antitumor activity against different cell lines, including the human colon cancer HCT-15 cell lines. A great inhibition of the breast cancer MCF7 and melanoma cancer MDA-MB-435 cell lines is achieved by the introduction of a basic piperidine unit as the substituent X. It is assumed that this derivative of hydantoin is located well in the biological target.

#### Crystal structures of **2a**, **2e**, and **2g**

The molecular structures of the compounds **2a**, **2e**, and **2g** are shown in Fig. 3. The bond distances and angles are as expected for hydantoin derivatives and are very similar mutually (Table 1). Also, the bond distances are in good accordance with the values calculated by DFT (Table 1). Four chemically identical, but crystallographically different molecules, A, B, C, and D, exist in the asymmetric unit of **2e** (Fig. 3). It is interesting to note that the orientation of the A, B, and D molecules are nearly the same, while the molecule C is in the opposite direction.

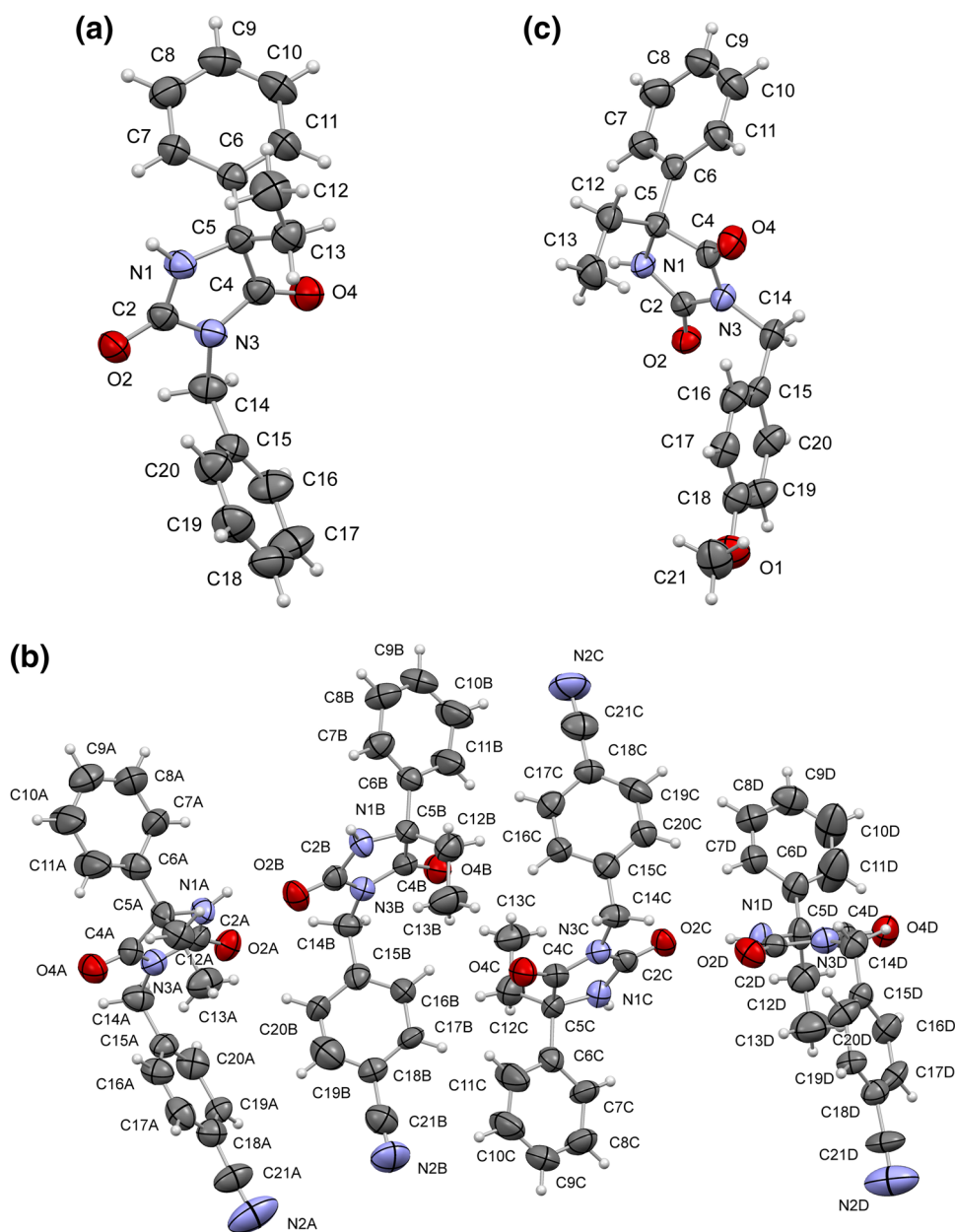
The general structural feature of **2a**, **2e**, and **2g** is that of crystal packing governed by only one hydrogen N–H...O bond in each case (Table 2) and numerous weak C–H...N/O contacts between neighboring molecules that stabilize the crystal lattices. In **2a**, hydrogen bonds between a pair of enantiomers make  $R_2^2(8)$  centrosymmetric dimers (Fig. 4a). The dimers further built double-layers parallel to the *ab*-plane that are linked by C–H...N/O and van der Waals interactions. The existence of centrosymmetric dimers in the crystal packing of **2a** may well influence differences in its pharmacokinetic properties, when compared with **2e** and **2g**.

Four crystallographically different molecules of **2e**, A, B, C, and D, make two pairs of zigzag chains parallel to the *c*-axis in the crystal packing (Fig. 5). In one pair, A and B (an enantiomeric pair), and in another, C and D molecules are connected through N–H...O hydrogen bonds (Table 2). A pair of zigzag chains formed by one stereoisomer parallel to the *b*-axis (Fig. 6) exists in **2g**.

#### Quantum chemical calculations

The geometry of the investigated compounds was optimized according to density functional theory (DFT) using B3LYP/6-311G(d,p) level, and selected geometric parameters are listed in Tables 1 and 3. The bonds in the hydantoin ring change very slightly upon changing the substituents R and X. The N1–C5 and C4–C5 single bonds in the molecules from series 1 are longer than those in the molecules from series 2 (about 0.010 and 0.005 Å, respectively). The N1–C2 and N3–C4 bond lengths of around 1.37 Å exhibit double-bond character and indicate strong stabilizing conjugation of the N1 and N3 atoms with the carbonyl groups. In the connecting chain, the N2–C14 bond becomes slightly longer with increasing electron-

**Fig. 3** ORTEP-like representations of asymmetric unit of the compounds: **2a** (a), **2e** (b), and **2g** (c) with atomic numbering schemes. Displacement ellipsoids are drawn at the 50 % probability level and the H atoms are shown as *small spheres* of arbitrary radii



donating ability of the benzyl substituent X, while the opposite is observed for the C14–C15 bond. With exception of **2g**, the values of torsion angle C4–C5–C6–C7 in the molecules from series **1** are about  $10^\circ$  smaller than those in the molecules from series **2**. This should be ascribed to the steric hindrance when two phenyl groups neighbor each other.

The selected structural parameters of the experimental crystal structures for compounds **2a**, **2e**, and **2g** are also compared with computed geometries in Table 1. The main differences between the experimental structures and structures computed by the DFT method result from the different spatial orientation of the phenyl and benzyl groups relative to the hydantoin moiety. The solid-state

structures of the investigated compounds can easily be affected by packing effects, which modify the geometry [12]. Thus, the conformation observed in the single crystal may differ from that at the biological target site.

The molecular orbital calculation of the investigated hydantoin derivatives has also been performed according to DFT. The energy of HOMO and LUMO are respectively a rough measure of the electron-donating and electron-withdrawing ability of a molecule [13]. Changing the substituents R and X modifies the energy gap between the HOMO and LUMO localized on different parts of the molecular skeleton (Table 4; Figs. 7, 8). According to the calculations, the electron density of the HOMO for the compounds **1a**, **1c**, **2a**, and **2c** spreads over the whole

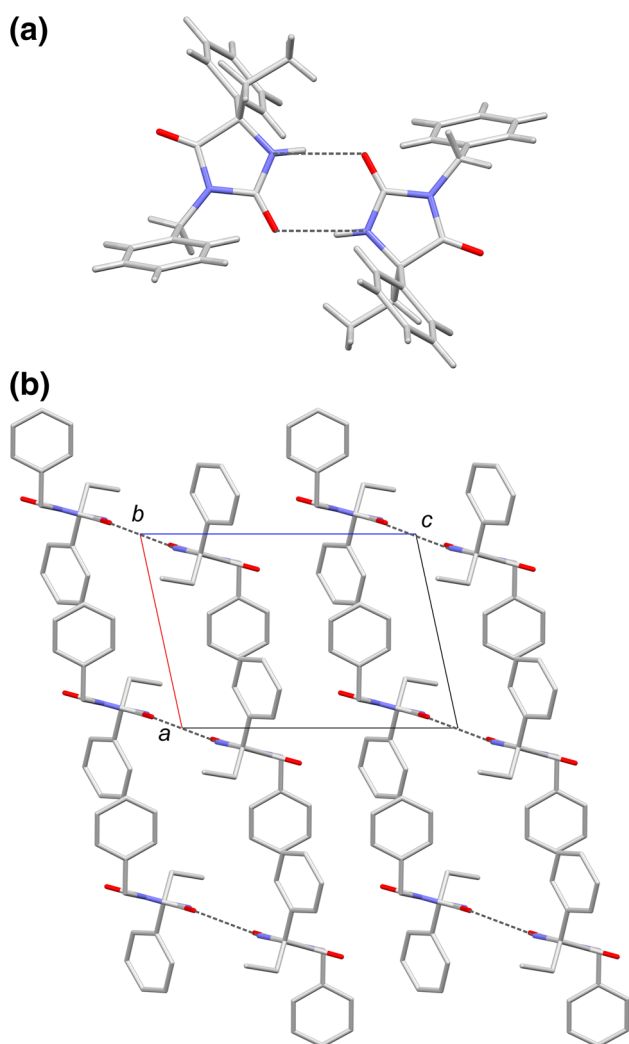
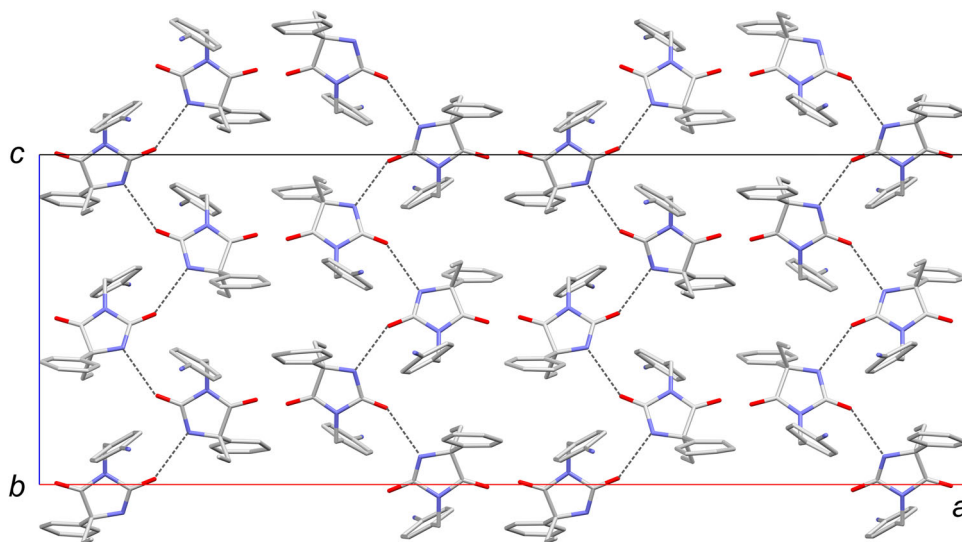


**Fig. 4** **a** Centrosymmetric dimers in **2a**; **b** crystal packing of compound **2a** showing layers parallel to the *ab*-plane. Intermolecular H bonds are represented by *dashed lines*

**Fig. 5** Crystal packing of compound **2e** viewed along *b*-axes. Intermolecular H bonds are represented by *dashed lines*



molecule, while the electron density of the LUMO is shifted toward the central hydantoin moiety and the phenyl group(s) in position 5. When substituent X is an electron-donating type, the HOMO is mostly localized on the benzyl moiety and the LUMO is to a large extent delocalized over the hydantoin and phenyl rings. When X is a strong electron-withdrawing substituent, the molecular orbital diagram is considerably different; the HOMO is mostly localized on the phenyl group(s) in position 5, while the LUMO is on the benzyl acceptor moiety (compounds **1f** and **2f**).

As expected, the electron-donating substituents X lead to high-lying HOMO, the highest energy being obtained for X = OCH<sub>3</sub> in both series of compounds, while electron-withdrawing substituents lead to low-lying LUMOs, the lowest energy being when X = NO<sub>2</sub>. The replacement of one of the phenyl groups in position 5 with an ethyl group leads to the stabilization of the LUMO for compounds **2a–2d** and **2g** with respect to the corresponding derivatives from series **1**. The energy of HOMO remains almost unchanged. On the other hand, the HOMO level for compounds **2e** and **2f** is stabilized when compared with the HOMO for **1e** and **1f**, while the energy of the LUMO is almost unaffected. The net result is that the HOMO–LUMO energy gap is somewhat smaller (by ~0.10 eV) for the compounds in series **1** than for the compounds in series **2**.

#### NBO analysis

A useful feature of the NBO method is that it gives information about interactions in both filled and virtual orbital spaces that can improve the analysis of intra- and intermolecular interactions. Delocalization of electron density between occupied Lewis-type (bonding or lone pair) NBO orbitals and formally unoccupied (anti-bonding

**Fig. 6** Zigzag chains parallel to *b*-axes in the crystal packing of compound **2g**. Intermolecular H bonds are represented by *dashed lines*

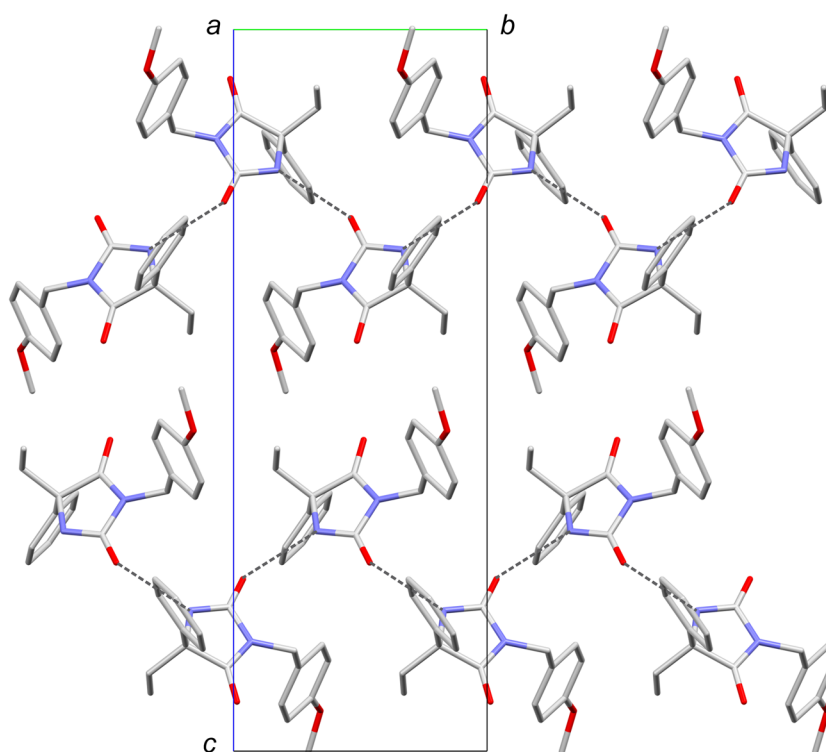


**Table 1** Selected structural parameters (bond distances/Å and torsion angles/°) obtained by theoretical calculations and single-crystal X-ray study for the investigated hydantoins **2a–2g**

	<b>2a</b> (X-ray)	<b>2a</b>	<b>2b</b>	<b>2c</b>	<b>2d</b>	<b>2e*</b> (X-ray)	<b>2e</b>	<b>2f</b>	<b>2g</b> (X-ray)	<b>2g</b>
N1–C2	1.334(2)	1.368	1.368	1.366	1.367	1.334	1.365	1.365	1.340(2)	1.368
N1–C5	1.461(2)	1.459	1.459	1.459	1.460	1.447	1.460	1.460	1.462(2)	1.458
C2–O2	1.229(2)	1.209	1.209	1.209	1.209	1.221	1.209	1.209	1.221(2)	1.209
C2–N3	1.395(2)	1.412	1.412	1.413	1.413	1.394	1.414	1.414	1.397(2)	1.412
N3–C4	1.372(2)	1.374	1.373	1.374	1.374	1.362	1.375	1.375	1.371(2)	1.373
C4–O4	1.207(2)	1.210	1.210	1.210	1.210	1.217	1.210	1.210	1.208(2)	1.211
C4–C5	1.541(2)	1.552	1.552	1.552	1.552	1.538	1.551	1.551	1.530(2)	1.552
N3–C14	1.462(2)	1.465	1.466	1.464	1.464	1.466	1.462	1.462	1.466(2)	1.467
C14–C15	1.509(2)	1.516	1.515	1.515	1.515	1.502	1.516	1.517	1.508(2)	1.513
C4–N3–C14–C15	94.0(2)	86.4	85.7	86.6	85.9	97.4	86.8	87.1	100.8(2)	86.5
N3–C14–C15–C16	135.2(2)**	87.9	87.7	85.9	86.1	62.8	85.6	85.8	63.5(2)**	90.2
N1–C5–C6–C7	−2.2(2)	−9.3	−9.6	−9.4	−8.5	−13.3	−9.2	−9.5	−42.0(2)**	−9.8
C4–C5–C6–C7	108.7(1)	120.5	120.9	120.6	119.7	125.4	120.4	120.6	152.3(1)	121.1

\* Bond distances are calculated as mean values of distances in individual A, B, C, and D molecules. Torsion angles are calculated as mean values of angles using the corresponding absolute values in A, B, C, and D molecules. The negative sign of the mean N1–C5–C6–C7 torsion angle is assigned according to the matching enantiomer

\*\* The sign of the torsion angle is selected according to the matching enantiomer

or Rydberg) non-Lewis NBO orbitals corresponds to a stabilizing donor–acceptor interaction. The larger the  $E(2)$  (energy of hyperconjugative interactions) value, the more intensive is the interaction between electron donors and electron acceptors.

NBO analysis has been performed on the molecule **2a** at the DFT level in order to elucidate the intramolecular interactions and delocalization of electron density within the

molecule. The intramolecular interactions are formed by the orbital overlap between bonding C–C, C–N, C–H, and C=O antibonding orbital, which results in intramolecular charge transfer (ICT) causing stabilization of the molecule. These interactions are observed due to an increase in the electron density (ED) in C–C, C–N, C–H, and C=O antibonding orbitals that weakens the respective bonds. The strong intramolecular hyperconjugative interaction of the  $\sigma$  and  $\pi$

**Table 2** Hydrogen bond geometry in **2a**, **2e**, and **2g**

D–H...A	$d(\text{D–H})/\text{\AA}$	$d(\text{H...A})/\text{\AA}$	$d(\text{D...A})/\text{\AA}$	$\angle(\text{DHA})/^\circ$
<b>2a</b>				
N1–H1...O2 <sup>a</sup>	0.93	1.92	2.837(2)	170
<b>2e</b>				
N1A–H1...O2B	0.86	2.17	2.847(6)	136
N1B–H18...O2A <sup>b</sup>	0.86	1.98	2.837(5)	171
N1C–H35...O2D <sup>c</sup>	0.86	2.05	2.764(6)	140
N1D–H52...O2C	0.86	2.09	2.931(6)	167
<b>2g</b>				
N1–H1...O2 <sup>d</sup>	0.86	2.07	2.900(2)	165

Symmetry codes: <sup>a</sup>  $-x, -y + 1, -z$ ; <sup>b</sup>  $x, -y + 1/2, z + 1/2$ ; <sup>c</sup>  $x, -y + 3/2, z - 1/2$ ; <sup>d</sup>  $-x + 2, y - 1/2, -z + 3/2$

**Table 3** Selected structural parameters (bond distances/ $\text{\AA}$  and torsion angles/ $^\circ$ ) obtained by theoretical calculations for the investigated hydantoins **1a–1h**

	<b>1a</b>	<b>1b</b>	<b>1c</b>	<b>1d</b>	<b>1e</b>	<b>1f</b>	<b>1g</b>	<b>1h</b>
N1–C2	1.372	1.372	1.371	1.371	1.369	1.369	1.373	1.372
N1–C5	1.469	1.469	1.469	1.469	1.470	1.470	1.469	1.468
C2–O2	1.209	1.209	1.209	1.209	1.209	1.209	1.209	1.209
C2–N3	1.410	1.409	1.410	1.411	1.411	1.411	1.409	1.410
N3–C4	1.374	1.373	1.374	1.374	1.375	1.375	1.373	1.374
C4–O4	1.208	1.208	1.208	1.208	1.208	1.208	1.208	1.208
C4–C5	1.557	1.558	1.558	1.558	1.557	1.557	1.559	1.558
N3–C14	1.466	1.467	1.465	1.464	1.462	1.462	1.468	1.467
C14–C15	1.516	1.515	1.515	1.516	1.516	1.517	1.514	1.515
C4–N3–C14–C15	84.8	85.5	86.6	85.8	86.7	87.2	85.6	86.4
N3–C14–C15–C16	83.7	83.8	83.8	85.0	82.7	83.0	86.5	86.2
N1–C5–C6–C7	–2.9	–2.7	–2.2	–1.3	–3.1	–2.9	–0.9	–1.0
C4–C5–C6–C7	107.3	107.6	107.9	108.8	107.0	107.2	109.2	109.1

electrons of C–C to the anti C–C bond of the hydantoin ring leads to stabilization of some part of the ring, as evident from Table S3 (Supplementary material). For example: the intramolecular hyperconjugative interaction of  $\sigma(\text{C4–N3})$  distributes to  $\sigma^*(\text{N3–C2})$ , C2–O2, and N1–C5, leading to stabilization of 2.85–4.48  $\text{kJ mol}^{-1}$ . The same kind of interaction is calculated in the  $\sigma$ -type bonding of C4–C5 with  $\sigma$ -type antibonding of C5–C6, N3–C14, and N1–H orbitals, as shown in Table S3.

The interaction energy, related to the resonance in the molecule, is electrons withdrawing to the ring through  $\sigma^*$  of N3–C2, C2–N1 and C4–N3, and the C4–C5 bond from the lone pairs LP(2)O2 and LP(2)O4, respectively, which leads to moderate stabilization energy of 92–109  $\text{kJ mol}^{-1}$  (Table S3). The most important interaction energies of lone pairs LP(1)N1  $\rightarrow \pi^*(\text{C2–O2})$ , LP(1)N3  $\rightarrow \pi^*(\text{C2–O2})$ , and LP(1)N3  $\rightarrow \pi^*(\text{C4–O4})$ , are 241.83, 206.91, and 248.48  $\text{kJ mol}^{-1}$ , respectively.

NBO analysis clearly manifests the evidences of the intramolecular charge transfer in molecule **2a** from  $\pi(\text{C–C})$  and  $\pi^*(\text{C–C})$  in the phenyl ring in position 5 and the phenyl ring of the benzyl moiety, as shown in Table S3, that clearly shows a large stabilization energy of about 84  $\text{kJ mol}^{-1}$ . The maximum energy delocalization takes place in the  $\pi$ – $\pi^*$  transition. The orbital overlap in phenyl rings between  $\pi(\text{C–C})$  and  $\pi^*(\text{C–C})$  results in an intramolecular charge transfer causing stabilization of the whole system.

#### Rule of five and drug-like properties

To identify which of the investigated compounds should be examined in detail, their drug-like properties have been considered based on the ‘rule of five’, as well as the number of rotatable bonds and polar surface area (Table 5). This empirical rule states that if a compound satisfies any two of the following rules, it is likely to exhibit poor in vivo

permeability: (1) molecular weight  $>500$ , (2) number of hydrogen bond donors  $>5$ , (3) number of hydrogen bond acceptors  $>10$ , and (4) calculated value of the logarithm of the octanol–water partition coefficient,  $\log P > 5$  [14]. In addition, reduced molecular flexibility (the number of rotatable bonds  $<8$ ) and low polar surface area ( $<140 \text{ \AA}^2$ ) are important predictors of good bioavailability [12, 15].

The investigated hydantoin derivatives are highly lipophilic compounds with lipophilicity between 3.36 and 6.12. A trend is observed: the strong electron-donating and electron-withdrawing groups (i.e.,  $\text{NO}_2$ ,  $\text{CN}$ ,  $\text{OCH}_3$ ) decrease lipophilicity, while the introduction of an alkyl or

halogen substituents yields the highest values. As expected, the replacement of one of the phenyl groups in position 5 with an ethyl group results in a decreased lipophilicity of compounds in series **2** with respect to the corresponding derivatives in series **1**. Generally, lipophilicity (expressed as  $\log P$ ) is directly related to the change in the Gibbs energy of solvation of a molecule between octanol and water; its dipolarity/polarizability and, especially, hydrogen bond basicity favor partitioning into water and thus decrease lipophilicity, whereas molecular size favors octanol [16, 17]. In a previous paper [18], we have shown that a linear dependency exists between  $\log P$  values and hydrogen bond basicity for the derivatives bearing moderate electron-donating and electron-withdrawing substituents X at the benzyl moiety (**1a–1d**, **1g**, **2a–2d**), whereas a strong electron-withdrawing substituent (**1f** and **2f**) significantly modifies the solvation characteristics of the molecule. It might be stated that more lipophilic compounds show higher inhibition, namely an increase in the antiproliferative activity is observed for compounds **1b**, **1c**, and **1d** with  $\log P$  in a range from 4.69 to 5.25. Furthermore, the investigated compounds contain a moderate number of the rotatable bonds, and thus somewhat larger conformational changes upon binding to a receptor are possible. A larger polar surface area indicates that reduced absorption can be expected. Evidently, the investigated hydantoin derivatives meet these empirical criteria and potentially qualify for the pharmacodynamic phase of the drug development.

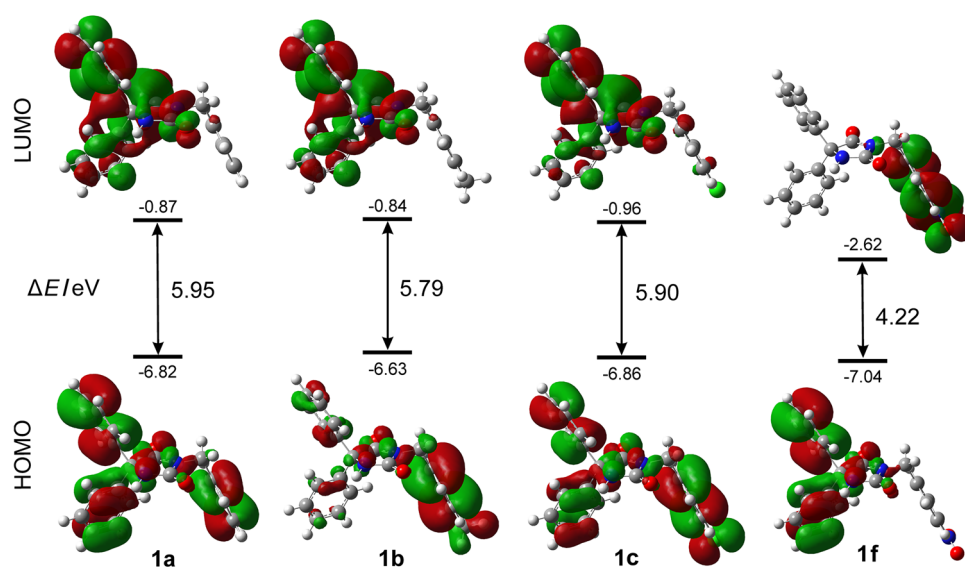
**Table 4** B3LYP/6-311G(d,p) HOMO and LUMO energies of the investigated hydantoin

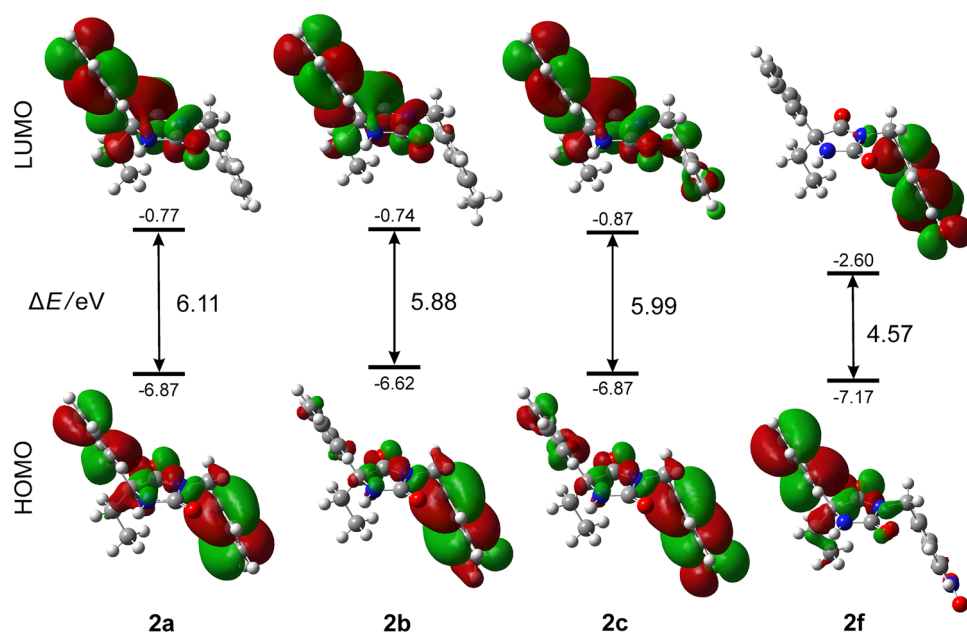
Compound	$E(\text{HOMO})/\text{eV}$	$E(\text{LUMO})/\text{eV}$	$E(\text{HOMO}) - E(\text{LUMO})/\text{eV}$
<b>1a</b>	-6.82	-0.87	5.95
<b>1b</b>	-6.63	-0.84	5.79
<b>1c</b>	-6.86	-0.96	5.90
<b>1d</b>	-6.79	-0.95	5.84
<b>1e</b>	-7.02	-1.73	5.29
<b>1f</b>	-7.04	-2.62	4.42
<b>1g</b>	-6.14	-0.81	5.34
<b>1h</b>	-6.64	-0.83	5.82
<b>2a</b>	-6.87	-0.77	6.11
<b>2b</b>	-6.62	-0.74	5.88
<b>2c</b>	-6.87	-0.87	5.99
<b>2d</b>	-6.77	-0.87	5.90
<b>2e</b>	-7.14	-1.71	5.43
<b>2f</b>	-7.17	-2.60	4.57
<b>2g</b>	-6.11	-0.72	5.38

## Conclusion

In this study, two new series of hydantoin derivatives were prepared and characterized. The in vitro antiproliferative

**Fig. 7** The molecular orbitals and HOMO–LUMO energy gaps for **1a**, **1b**, **1c**, and **1f**



**Fig. 8** The molecular orbitals and HOMO–LUMO energy gaps for **2a**, **2b**, **2c**, and **2f****Table 5** Evaluation of drug candidates

Compound	Molecular weight	Clog <i>P</i>	Hydrogen bonds		Rotatable bonds	Polar surface area/Å <sup>2</sup>	Violations
			Donors <sup>a</sup>	Acceptors <sup>b</sup>			
<b>1a</b>	342.39	4.41	1	4	4	69.26	0
<b>1b</b>	356.42	4.69	1	4	4	68.17	0
<b>1c</b>	376.84	4.97	1	4	4	68.61	0
<b>1d</b>	421.29	5.24	1	4	4	68.97	1
<b>1e</b>	367.40	4.55	1	5	4	124.9	0
<b>1f</b>	387.39	4.45	1	7	5	161.9	1
<b>1g</b>	372.42	4.13	1	5	5	85.08	0
<b>1h</b>	398.50	6.12	1	4	5	68.48	1
<b>2a</b>	294.34	3.64	1	4	4	68.07	0
<b>2b</b>	308.37	3.92	1	4	4	68.20	0
<b>2c</b>	328.79	4.20	1	4	4	68.20	0
<b>2d</b>	373.24	4.47	1	4	4	68.33	0
<b>2e</b>	319.36	3.78	1	5	4	126.2	0
<b>2f</b>	339.35	3.68	1	7	5	159.9	1
<b>2g</b>	324.37	3.36	1	5	5	84.92	0
Ideal compound	<500	<5	<5	<10	<8	<140	≤1

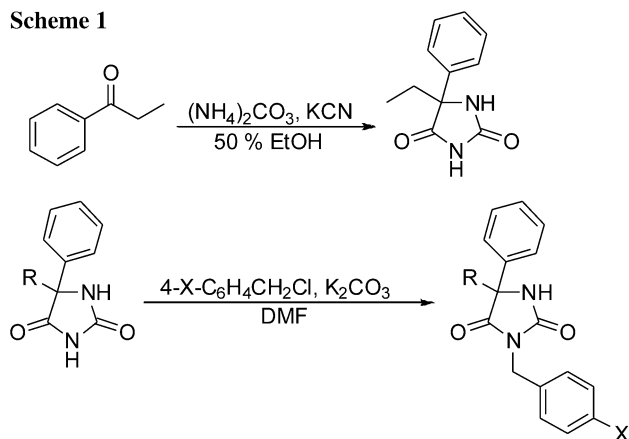
<sup>a</sup> A donor indicates any O–H or N–H group

<sup>b</sup> An acceptor indicates any O or N including those in donor groups

activity of the investigated hydantoin derivatives was evaluated against two human cancer cell lines: HCT-116 (colon carcinoma) and MDA-MB-231 (breast cancer). Most of the investigated compounds show superior anti-proliferative activity against MDA-MB-231 than against HCT-116 cell line, whereby those in series **1** possess higher potencies than the compounds in series **2**.

The crystal structure of compounds **2a**, **2e**, and **2g** was resolved by X-ray diffraction. Crystal packings are mainly governed by hydrogen N–H···O bonds between neighboring molecules. In **2a**, hydrogen bonds make R<sub>2</sub><sup>2</sup>(8) centrosymmetric dimers along the *c*-axis. In other two compounds, N–H···O bonds between neighboring molecules built zigzag chains connected further by van der Waals forces only.

Scheme 1



DFT calculations were used to obtain the molecular geometries and bonding features of the investigated compounds. The main differences between the experimental structures and computed geometries result from the different orientation of the phenyl and benzyl groups relative to the hydantoin moiety. This can be attributed to the packing effects that influence the conformation of real molecules. A detailed analysis of the effect of substituents on both hydantoin and benzyl moieties on the frontier molecular orbitals was also performed.

By assessing their different physicochemical properties, guidelines for the design of further derivatives were achieved. Regarding the biological profile, compounds **1b**, **1c**, and **1d** represent starting points for the development of new, specific antiproliferative hydantoins. Further studies should also examine their antiproliferative potential against additional cell lines.

## Materials and methods

### Synthesis

Commercially available materials were used without further purification. The investigated hydantoin derivatives were synthesized following the procedure presented in the synthesis scheme (Scheme 1). Phenytoin was commercially available, while 5-ethyl-5-phenylhydantoin was synthesized according to the method of Bucherer and Lieb [19]. The investigated compounds were obtained in the reaction between the starting hydantoins and 4-substituted benzyl chlorides in the presence of K<sub>2</sub>CO<sub>3</sub>, as described previously [20].

The chemical structures and the purities of the synthesized hydantoin derivatives were confirmed by melting points, elemental analysis, FT-IR, <sup>1</sup>H and <sup>13</sup>C NMR spectra, and agree well with the reported data (Table 6). Herein, the characterization of **1e**, **1g**, **1h**, **2e**, and **2g** as novel

Table 6 Synthesis of the investigated hydantoin derivatives

Compound	Yield/%	M.p./°C	
		Found	Reported
<b>1a</b>	49	145–146	145–146 [21]
<b>1b</b>	55	110–112	110–112 [18]
<b>1c</b>	48	140–142	140–142 [18]
<b>1d</b>	52	130–133	130–133 [18]
<b>1e</b>	48	98–100	–
<b>1f</b>	42	174–177	174–177 [18]
<b>1g</b>	56	122–125	–
<b>1h</b>	50	142–144	–
<b>2a</b>	62	138–140	138–140 [22]
<b>2b</b>	56	164–167	164–167 [18]
<b>2c</b>	68	165–168	165–168 [18]
<b>2d</b>	72	170–173	170–173 [18]
<b>2e</b>	58	141–143	–
<b>2f</b>	68	174–176	174–176 [18]
<b>2g</b>	74	147–149	–

derivatives is presented. Elemental analysis was realized using an Elemental Vario EL III microanalyzer, and the results were found to be in good agreement ( $\pm 0.3\%$ ) with the calculated values. FT-IR spectra were recorded on a Bomem MB 100 spectrometer in the form of KBr pellets. <sup>1</sup>H and <sup>13</sup>C NMR spectra were recorded on a Varian Gemini 200 spectrometer at 200 MHz for the <sup>1</sup>H NMR and 50 MHz for the <sup>13</sup>C NMR spectra. The spectra were recorded at room temperature in CDCl<sub>3</sub> and DMSO-*d*<sub>6</sub>. The chemical shifts are expressed in ppm, referring to TMS ( $\delta(\text{H}) = 0$  ppm) in the <sup>1</sup>H NMR and the residual solvent signal (CDCl<sub>3</sub>:  $\delta(\text{C}) = 77$  ppm; DMSO-*d*<sub>6</sub>:  $\delta(\text{C}) = 39.5$  ppm) in the <sup>13</sup>C NMR spectra. The coupling constants *J*(H,H) are expressed in Hz.

### 4-[(2,5-Dioxo-4,4-diphenyl-1-imidazolidinyl)methyl]-benzotrile (**1e**, C<sub>23</sub>H<sub>17</sub>N<sub>3</sub>O<sub>2</sub>)

White crystalline solid; yield: 48 %; m.p.: 98–100 °C; IR (KBr):  $\bar{\nu} = 3,248$  (NH), 1,748 (C=O), 1,706 (C=O) cm<sup>-1</sup>; <sup>1</sup>H NMR (200 MHz, DMSO-*d*<sub>6</sub>):  $\delta = 9.88$  (s, 1H, NH), 7.78 (d, 2H, *J* = 8 Hz, -C<sub>6</sub>H<sub>4</sub>-), 7.40 (d, 2H, *J* = 8 Hz, -C<sub>6</sub>H<sub>4</sub>-), 7.40–7.30 (m, 10H, 2 × C<sub>6</sub>H<sub>5</sub>), 4.75 (s, 2H, N-CH<sub>2</sub>-) ppm; <sup>13</sup>C NMR (50 MHz, DMSO-*d*<sub>6</sub>):  $\delta = 173.3$  (C4), 155.3 (C2), 142.3, 139.7, 132.9, 129.0, 128.6, 128.5, 126.9, 118.9, 110.8, 69.7 (C5), 41.5 ppm.

### 3-(4-Methoxybenzyl)-5,5-diphenyl-2,4-imidazolidinedione (**1g**, C<sub>23</sub>H<sub>20</sub>N<sub>2</sub>O<sub>3</sub>)

White crystalline solid; yield: 56 %; m.p.: 122–125 °C; IR (KBr):  $\bar{\nu} = 3,339$  (NH), 1,765 (C=O), 1,706 (C=O) cm<sup>-1</sup>; <sup>1</sup>H NMR (200 MHz, DMSO-*d*<sub>6</sub>):  $\delta = 9.73$  (s, 1H, NH), 7.43–7.30 (m, 10H, 2 × C<sub>6</sub>H<sub>5</sub>), 7.18 (d, 2H, *J* = 8 Hz,

–C<sub>6</sub>H<sub>4</sub>–), 6.87 (d, 2H, *J* = 8 Hz, –C<sub>6</sub>H<sub>4</sub>–), 4.56 (s, 2H, N–CH<sub>2</sub>–), 3.70 (s, 3H, –OCH<sub>3</sub>) ppm; <sup>13</sup>C NMR (50 MHz, DMSO-*d*<sub>6</sub>): δ = 173.3 (C4), 158.9, 155.5 (C2), 139.9, 129.2, 128.9, 128.8, 128.5, 126.8, 114.2, 69.4 (C5), 55.3, 41.2 ppm.

*3-(4-tert-Butylbenzyl)-5,5-diphenyl-2,4-imidazolidinedione (1h, C<sub>26</sub>H<sub>26</sub>N<sub>2</sub>O<sub>2</sub>)*

White crystalline solid; yield: 50 %; m.p.: 142–144 °C; IR (KBr):  $\bar{\nu}$  = 3,260 (NH), 1,771 (C=O), 1,713 (C=O) cm<sup>-1</sup>; <sup>1</sup>H NMR (200 MHz, DMSO-*d*<sub>6</sub>): δ = 9.72 (s, 1H, NH), 7.44–7.35 (m, 10H, 2 × C<sub>6</sub>H<sub>5</sub>), 7.33 (d, 2H, *J* = 8.6 Hz, –C<sub>6</sub>H<sub>4</sub>–), 7.16 (d, 2H, *J* = 8.6 Hz, –C<sub>6</sub>H<sub>4</sub>–), 4.61 (s, 2H, N–CH<sub>2</sub>–), 1.23 (s, 9H, C(CH<sub>3</sub>)<sub>3</sub>) ppm; <sup>13</sup>C NMR (50 MHz, DMSO-*d*<sub>6</sub>): δ = 173.3 (C4), 155.5 (C2), 150.2, 139.9, 133.8, 128.8, 128.4, 127.2, 126.8, 69.4 (C5), 41.4, 34.4, 31.3 ppm.

*4-[(4-Ethyl-2,5-dioxo-4-phenyl-1-imidazolidinyl)methyl]benzonitrile (2e, C<sub>19</sub>H<sub>17</sub>N<sub>3</sub>O<sub>2</sub>)*

White crystalline solid; yield: 58 %; m.p.: 141–143 °C; IR (KBr):  $\bar{\nu}$  = 3,259 (NH), 1,759 (C=O), 1,709 (C=O) cm<sup>-1</sup>; <sup>1</sup>H NMR (200 MHz, DMSO-*d*<sub>6</sub>): δ = 9.21 (s, 1H, NH), 7.81 (d, 2H, *J* = 7.8 Hz, –C<sub>6</sub>H<sub>4</sub>–), 7.54 (d, 2H, *J* = 7.8 Hz, –C<sub>6</sub>H<sub>4</sub>–), 7.46–7.31 (m, 5H, C<sub>6</sub>H<sub>5</sub>), 4.67 (s, 2H, N–CH<sub>2</sub>–), 2.24–1.90 (m, 2H, –CH<sub>2</sub>–), 0.78 (t, 3H, *J* = 7.3 Hz, –CH<sub>3</sub>) ppm; <sup>13</sup>C NMR (50 MHz, DMSO-*d*<sub>6</sub>): δ = 174.8 (C4), 156.0 (C2), 142.4, 138.7, 132.8, 128.9, 128.5, 128.3, 125.7, 118.9, 110.7, 67.4 (C5), 41.2, 31.6, 8.2 ppm.

*5-Ethyl-3-(4-methoxybenzyl)-5-phenyl-2,4-imidazolidinedione (2g, C<sub>19</sub>H<sub>20</sub>N<sub>2</sub>O<sub>3</sub>)*

White crystalline solid; yield: 74 %; m.p.: 147–149 °C; IR (KBr):  $\bar{\nu}$  = 3,269 (NH), 1,765 (C=O), 1,706 (C=O) cm<sup>-1</sup>; <sup>1</sup>H NMR (200 MHz, DMSO-*d*<sub>6</sub>): δ = 9.07 (s, 1H, NH), 7.54–7.31 (m, 5H, C<sub>6</sub>H<sub>5</sub>), 7.18 (d, 2H, *J* = 8 Hz, –C<sub>6</sub>H<sub>4</sub>–), 6.86 (d, 2H, *J* = 8 Hz, –C<sub>6</sub>H<sub>4</sub>–), 4.48 (s, 2H, N–CH<sub>2</sub>–), 3.70 (s, 3H, –OCH<sub>3</sub>), 2.16–1.89 (m, 2H, –CH<sub>2</sub>–), 0.73 (t, 3H, *J* = 7.3 Hz, –CH<sub>3</sub>) ppm; <sup>13</sup>C NMR (50 MHz, DMSO-*d*<sub>6</sub>): δ = 174.7 (C4), 158.9, 156.2 (C2), 139.0, 129.3, 129.0, 128.8, 128.2, 125.7, 114.1, 67.1 (C5), 55.2, 41.0, 31.7, 8.1 ppm.

*Crystal structure determination*

Single crystals of **2a**, **2e**, and **2g** were obtained by slow evaporation (30 days at –5 °C) from a diluted ethanol (**2a**) or ethyl acetate solution (**2e** and **2g**). Suitable colorless, single crystals of **2a**, **2e**, and **2g** were chosen for the structure determination. X-ray single-crystal diffraction data were collected on an Oxford Gemini S diffractometer equipped with a CCD detector at 293(2) K. In the case of single-crystal **2a**, monochromatized Mo K $\alpha$  radiation

( $\lambda$  = 0.71073 Å) was used, while Cu K $\alpha$  radiation ( $\lambda$  = 1.5418 Å) was applied for single-crystals **2e** and **2g**. A multi-scan correction for absorption was applied in all cases. The structures were solved by direct methods (SIR92 [23] for **2a** and **2g** and SIR2004 [24] for **2e**) and refined on *F*<sup>2</sup> by full-matrix least-squares using the programs SHELXL97 [25] and WinGX [26]. For all three compounds, non-hydrogen atoms were refined anisotropically. Hydrogen atoms were placed at geometrically calculated positions and refined using a riding model with fixed C–H and N–H distances. A test of intensity statistics indicated that the selected crystal of **2e** was a pseudo-merohedral twin with a twin law (1 0 0/0 –1 0/0 0 –1). Therefore, a new reflection file (HKLF5) with detwinned data was generated using the program PLATON [27]. Selected crystallographic data and refinement results are listed in Table 7.

Crystallographic data for the structures in this paper were deposited in the Cambridge Crystallographic Data Centre as supplementary publication numbers CCDC 959932-959934. These data can be obtained free of charge from [http://www.ccdc.cam.ac.uk/data\\_request/cif](http://www.ccdc.cam.ac.uk/data_request/cif), by emailing [data\\_request@ccdc.cam.ac.uk](mailto:data_request@ccdc.cam.ac.uk), or by contacting the Cambridge Crystallographic Data Centre, 12, Union Road, Cambridge CB2 1EZ, UK; Fax: +44-1223-336033.

*Biological characterization*

*Compounds and solutions*

MTT was dissolved (5 mg cm<sup>-3</sup>) in phosphate buffered saline (pH 7.2) and filtered (0.22 μm) before use. The RPMI 1,640 cell culture medium, fetal bovine serum (FBS), and MTT were purchased from Sigma Chemical Company, USA.

*Cell lines*

Human colon cancer HCT-116 and human breast cancer MDA-MB-231 cell lines were maintained in a monolayer culture using a nutrient medium RPMI 1,640 with 10 % FBS and antibiotics.

*Treatment of peritoneal macrophages for evaluation of cytotoxic effect*

Stock solutions of compounds were prepared in DMSO and dissolved in the corresponding medium to the required working concentrations. The compounds were evaluated for their cytotoxic effects on rat peritoneal macrophages by the MTT assay during 24 h. Rat peritoneal macrophages (10,000 cells per well) were seeded into wells of a 96-well, flat-bottomed microtiter plate in 0.1 cm<sup>3</sup> of medium with or without LPS. After 24 h of incubation, 0.1 cm<sup>3</sup> of the investigated compound was added to cells in the final concentration (0.01, 0.1, 1, 10, 50, and 100 μmol dm<sup>-3</sup>), except in the control wells where only medium was added to the

**Table 7** Crystallographic data and structure refinement for compounds **2a**, **2e**, and **2g**

Compound	<b>2a</b>	<b>2e</b>	<b>2g</b>
Molecular formula	C <sub>18</sub> H <sub>18</sub> N <sub>2</sub> O <sub>2</sub>	C <sub>19</sub> H <sub>17</sub> N <sub>3</sub> O <sub>2</sub>	C <sub>19</sub> H <sub>20</sub> N <sub>2</sub> O <sub>3</sub>
<i>M</i> /g mol <sup>-1</sup>	294.34	319.36	324.37
Crystal system	Triclinic	Monoclinic	Monoclinic
Space group	<i>P</i> $\bar{1}$	<i>P</i> 2 <sub>1</sub> / <i>c</i>	<i>P</i> 2 <sub>1</sub> / <i>c</i>
<i>a</i> /Å	8.3857(2)	43.1188(8)	8.7665(4)
<i>b</i> /Å	8.8113(5)	10.1104(2)	8.1607(3)
<i>c</i> /Å	11.2005(8)	15.3109(3)	23.2077(9)
$\alpha$ /°	88.679(15)	90	90
$\beta$ /°	77.885(12)	90.002(5)	92.179(4)
$\gamma$ /°	74.171(11)	90	90
Crystal size/mm <sup>3</sup>	0.45 × 0.12 × 0.09	0.37 × 0.10 × 0.09	0.17 × 0.08 × 0.07
<i>V</i> /Å <sup>3</sup>	777.96(7)	6,674.8(2)	1,659.10(12)
<i>Z</i>	2	16	4
$\rho_c$ /g cm <sup>-3</sup>	1.257	1.271	1.299
$\mu$ /mm <sup>-1</sup>	0.083	0.682	0.718
<i>F</i> /000	312	2,687	688
$\theta$ range/°	1.86–25.68	5.02–70.07	3.81–70.06
Range of <i>h</i> , <i>k</i> , <i>l</i>	−10 ≤ <i>h</i> ≤ 9, −7 ≤ <i>k</i> ≤ 10, −13 ≤ <i>l</i> ≤ 12	−51 ≤ <i>h</i> ≤ 52, −4 ≤ <i>k</i> ≤ 12, −18 ≤ <i>l</i> ≤ 18	−9 ≤ <i>h</i> ≤ 10, −9 ≤ <i>k</i> ≤ 4, −27 ≤ <i>l</i> ≤ 28
Reflections collected/unique	7,405/2,912 ( <i>R</i> <sub>int</sub> = 0.0258)	38,960/12,623 ( <i>R</i> <sub>int</sub> = 0.0294)	5,690/3,141 ( <i>R</i> <sub>int</sub> = 0.0183)
Data/restraints/parameters	2,912/0/203	12,623/0/866	3,141/0/221
Observed <i>I</i> > 2σ( <i>I</i> ) reflections	2,174	8,413	2,545
<i>R</i> indices [ <i>I</i> > 2σ( <i>I</i> )]	<i>R</i> <sub>1</sub> = 0.0420, <i>wR</i> <sub>2</sub> = 0.1092 <sup>a</sup>	<i>R</i> <sub>1</sub> = 0.0987, <i>wR</i> <sub>2</sub> = 0.2808 <sup>b</sup>	<i>R</i> <sub>1</sub> = 0.0404, <i>wR</i> <sub>2</sub> = 0.1029 <sup>c</sup>
<i>R</i> indices (all data)	<i>R</i> <sub>1</sub> = 0.0577, <i>wR</i> <sub>2</sub> = 0.1178	<i>R</i> <sub>1</sub> = 0.1265, <i>wR</i> <sub>2</sub> = 0.3167	<i>R</i> <sub>1</sub> = 0.0514, <i>wR</i> <sub>2</sub> = 0.1102
<i>GOF</i> on <i>F</i> <sup>2</sup>	0.997	1.035	1.038
$\Delta\rho_{\max}$ , $\Delta\rho_{\min}$ /eÅ <sup>-3</sup>	0.174, −0.141	0.670, −0.283	0.162, −0.186

<sup>a</sup>  $w = 1/[\sigma^2(F_o^2) + (0.0685P)^2]$ , where  $P = (F_o^2 + 2F_c^2)/3$

<sup>b</sup>  $w = 1/[\sigma^2(F_o^2) + (0.1759P)^2 + 4.7267P]$ , where  $P = (F_o^2 + 2F_c^2)/3$

<sup>c</sup>  $w = 1/[\sigma^2(F_o^2) + (0.0489P)^2 + 0.2351P]$ , where  $P = (F_o^2 + 2F_c^2)/3$

cells. The effects of the investigated compounds on the survival of peritoneal macrophages was determined 24 h later by the MTT test [28], modified by Ohno and Abe [29]. Briefly, 0.02 cm<sup>3</sup> of MTT dye (5 mg cm<sup>-3</sup>) was added to each well. After incubation for further 3 h, 0.1 cm<sup>3</sup> of 10 % SDS (sodium dodecyl sulfate) was added to extract the insoluble product formazan resulting from conversion of the MTT dye by viable cells. The number of viable cells in each well is proportional to the intensity of the absorbance of light, which was then read in an ELISA plate reader at 570 nm.

#### Treatment of cell lines for antiproliferative in vitro screening

The target cells HCT-116 (10,000 cells per well) and MDA-MB-231 (100,000 cells per well) were seeded in triplicate into wells of a 96-well, flat-bottomed microtiter plate in 0.1 cm<sup>3</sup> medium. Twenty-four hours later, after the cell adaptation and adherence for both cell lines, 0.1 cm<sup>3</sup> of

the investigated compound was added to cells in the final concentration (0.01, 0.1, 1, 10, 50, and 100 μmol dm<sup>-3</sup>), except in the control wells, where only medium was added to the cells. The effect of the investigated compounds on cancer cell survival was determined 24 h later by the MTT test described in the previous section. The antiproliferative effect of the compounds was expressed as a percentage of inhibition of untreated cell proliferation. It was calculated as 100 % minus the ratio between the absorbance of each dose of the compounds and the absorbance of the untreated control cells × 100.

#### Computational details

The geometry of the investigated hydantoins was fully optimized with the DFT B3LYP/6-311G(d,p) method without any constraint on the geometry using Gaussian 09 program package [30]. The validity of the optimized

geometry was confirmed by frequency calculations, which gave real values for all the obtained frequencies. The frontier molecular orbital energies and HOMO–LUMO energy gaps were also calculated with the same methods.

Natural bond orbital (NBO) analysis [31] was performed using the NBO 3.1 program, as implemented in the Gaussian 09 package [30] at the B3LYP/6-311G(d,p) level in order to understand various second-order interactions between the filled orbitals of one subsystem and vacant orbitals of another subsystem, which is a measure of the intramolecular delocalization of electron density (ED). The second-order perturbation theory analysis of the Fock matrix in the NBO basis of molecule **2a** was carried out to evaluate the donor–acceptor interactions.

The optimized geometries from the DFT calculation were further used for the estimation of physicochemical descriptors (molecular mass, molecular volume, and polar surface area) by applying Vega ZZ version 2.4 [32].

**Acknowledgments** This work has been performed within the framework of the research projects Nos. ON 172013, III 45007, and ON 172035, supported by the Ministry of Education, Science and Technological Development of the Republic of Serbia.

## References

- Lemke TL, Williams DA (2008) Foye's principles of medicinal chemistry, 6th edn. Lippincott Williams and Wilkins, Philadelphia
- Shoemaker DD, O'Dwyer PJ, Marsoni S, Plowman J, Davignon JP, Davis RD (1983) *Invest New Drugs* 1:303
- Kassouf W, Tanguay S, Aprikian AG (2003) *J Urol* 169:1742
- Rajic Z, Zorc B, Raic-Malic S, Ester K, Kralj M, Pavelic K, Balzarini J, De Clercq E, Mintas M (2006) *Molecules* 11:837
- Ananda Kumar CS, Kavitha CV, Vinaya K, Prasad SBB, Thimmegowda NR, Chandrappa S, Raghavan SC, Rangappa KS (2009) *Invest New Drugs* 27:327
- Kavitha CV, Nambiar M, Ananda Kumar CS, Choudhary B, Muniyappa K, Rangappa KS, Raghavan SC (2009) *Biochem Pharmacol* 77:348
- Cavazzoni A, Alfieri RR, Carmi C, Zuliani V, Galetti M, Fumarola C, Frazzi R, Bonelli M, Bordi F, Lodola A, Mor M, Petronini PG (2008) *Mol Cancer Ther* 7:361
- Khanfar MA, El Sayed KA (2010) *Eur J Med Chem* 45:5397
- Abadi AH, Gary BD, Tinsley HN, Piazza GA, Abdel-Halim M (2010) *Eur J Med Chem* 45:1278
- Alanazi AM, El-Azab AS, Al-Swaidan IA, Maarouf AR, El-Bendary ER, Abu El-Enin MA, Abdel-Aziz AAM (2013) *Med Chem Res* 22:6129
- Trišović N, Božić B, Obradović A, Stefanović O, Marković S, Čomić LJ, Božić B, Ušćumlić G (2011) *J Serb Chem Soc* 76:1597
- Remko M, Swary M, Bickelhaupt FM (2006) *Bioorg Med Chem* 14:1715
- Bolognese A, Correale G, Manfra M, Lavecchia A, Mazzoni O, Novellino E, Barone V, La Colla P, Loddo R (2002) *J Med Chem* 45:5217
- Lipinski CA, Lombardo F, Dominy BW, Feeney PJ (1997) *Adv Drug Deliv Rev* 23:3
- Veber DF, Johnson SR, Cheng HY, Smith BR, Ward KW, Kopple KD (2002) *J Med Chem* 45:2615
- Abraham MH, Lieb WR, Franks NP (1991) *J Pharm Sci* 80:719
- Abraham MH (1993) *Pure Appl Chem* 65:2503
- Hmuda SH, Trišović NP, Valentić NV, Ušćumlić GS (2011) *J Solut Chem* 40:307
- Bucherer HT, Lieb VA (1934) *J Prakt Chem* 141:5
- Suzuki H, Kneller MB, Rock DA, Jones JP, Trager WF, Rettie AE (2004) *Arch Biochem Biophys* 429:1
- Hoffman C (1950) *Bull Soc Chim Fr* 45
- Fabrique de Produits Chimiques Ci-devant Sandoz (1934) Procédé de préparation de mono- et di-*n*-alcoyl- ou aralcoyl-5,5-phényl-éthylhydantoïnes FR 769667, 31 Aug 1934; (1935) *Chem Abstr* 29:12252
- Altomare A, Cascarano G, Giacovazzo C, Guagliardi A, Burla MC, Polidori G, Camalli M (1994) *J Appl Crystallogr* 27:435
- Burla MC, Caliandro R, Camalli M, Carrozzini B, Cascarano GL, De Caro L, Giacovazzo C, Polidori G, Spagna R (2005) *J Appl Crystallogr* 38:381
- Sheldrick GM (2008) *Acta Crystallogr A* 64:112
- Farrugia LJ (2012) *J Appl Crystallogr* 45:849
- Spek AL (2003) *J Appl Crystallogr* 36:7
- Mosmann T (1983) *J Immunol Methods* 65:55
- Ohno M, Abe T (1991) *J Immunol Methods* 145:199
- Frisch MJ, Trucks GW, Schlegel HB, Scuseria GE, Robb MA, Cheeseman JR, Scalmani G, Barone V, Mennucci B, Petersson GA, Nakatsuji H, Caricato M, Li X, Hratchian HP, Izmaylov AF, Bloino J, Zheng G, Sonnenberg JL, Hada M, Ehara M, Toyota K, Fukuda H, Hasegawa J, Ishida M, Nakajima T, Honda Y, Kitao O, Nakai H, Vreven T, Montgomery JA, Peralta JE Jr, Ogliaro F, Bearpark M, Heyd JJ, Brothers E, Kudin KN, Staroverov VN, Keith T, Kobayashi R, Normand J, Raghavachari K, Rendell A, Burant JC, Iyengar SS, Tomasi J, Cossi M, Rega N, Millam JM, Klene M, Knox JE, Cross JB, Bakken V, Adamo C, Jaramillo J, Gomperts R, Stratmann RE, Yazyev O, Austin AJ, Cammi R, Pomelli C, Ochterski JW, Martin RL, Morokuma K, Zakrzewski VG, Voth GA, Salvador P, Dannenberg JJ, Dapprich S, Daniels AD, Farkas O, Foresman JB, Ortiz JV, Cioslowski J, Fox DJ (2010) *Gaussian 09, Revision C.01*. Gaussian Inc, Wallingford
- Glendening ED, Reed AE, Carpenter JE, Weinhold F (1998) *NBO version 3.1*. TCI, University of Wisconsin, Madison
- Pedretti A, Villa L, Vistoli G (2004) *J Comput Aid Mol Des* 18:167